Investigation of a turbulent channel flow using large eddy simulation

F. Kremer[a], C. Bogey[a] and C. Bailly[b]

[a]Ecole Centrale de Lyon, Centre Acoustique, 36 Avenue Guy de Collongue, 69134 Ecully, France
[b]Laboratoire de Mecanique des Fluides et d'Acoustique, 36 Av Guy de Collongue 69134 Ecully Cedex
francois.kremer@ec-lyon.fr

Large-Eddy Simulations (LES) of a compressible turbulent channel flow at a Mach number of 0.5 and a friction Reynolds number of 260 are performed, using explicit low-dissipation and low-dispersion numerical schemes for spatial derivatives. Eleven simulations are carried out on grids with different mesh spacings in order to study the grid convergence of turbulence statistics, namely mean and fluctuating streamwise velocity profiles. These quantities are found to not vary significantly for mesh spacings smaller than 10 and 30 wall units in the spanwise and streamwise directions, respectively. An additional simulation is performed using a semi-implicit Runge-Kutta algorithm, developed specifically for wall-bounded flows, in which terms involving wall normal derivatives are integrated implicitly, while the other terms are integrated explicitly to relax the CFL constraint in the wall normal direction. The simulations finally provide a numerical database, from which wall pressure and velocity spectra are computed to give insights into the turbulent structures developing in the flow.

1 Introduction

Since the direct numerical simulation (DNS) by Kim *et al.* [1], the fully turbulent channel flow has been widely studied using computations because this configuration enables universal characteristics of wall turbulence to be studied, while offering a relative simplicity of implementation compared to other canonical wall-bounded flows such as the turbulent boundary layer [2]. However, some intrinsic difficulties of wall bounded flow remain for numerical simulation. The dynamics of the flow is indeed strongly influenced by the dynamics of the small scales developing close to the wall, which exhibit strong anisotropy and complex interaction mechanisms with larger scales. Thus, to properly catch the features of wall bounded flows, simulations must ensure a good resolution of these small scales.

This can be particularly tricky in large eddy simulation (LES), where scales are not taken into account by the grid resolution, and must be treated by a subgrid model. If the small scales mentioned above for wall-bounded flows are smaller than the mesh spaces, their specific behavior cannot be well reproduced, and important errors might occur, even on global features such as the mean velocity profile of the flow. A general assessment of the grid resolution is moreover difficult for LES, since many subgrid models exist, and may have different effects on the resolved scales. For this reason, a grid convergence study is carried out in the present study of a turbulent channel flow, in which the LES strategy relies on the use of a relaxation filter as proposed by Bogey *et al.* [3].

Well-resolved LESs allow fine investigation of turbulence structures developing near the wall. These structures have been studied for instance by Tomkins & Adrian [4] for boundary layers, and by Jiménez *et al.* [5] for channel flows. Both authors investigated the scaling of turbulent motions at different distances to the wall, from the inner layer to the logarithmic region. A study based on LES data has also been conducted by Bogey *et al.*, who simulated a tripped nozzle pipe flow [6]. They found that just downstream the nozzle exit, the azimuthal modes of streamwise velocity scale similarly to the spanwise modes in boundary layers [7].

Wall pressure spectra have also been studied in several analytical, experimental and numerical investigations over the last fifty years [8]. Among recent studies, Hu *et al.* [9] computed wall pressure spectra using DNS for channel flows at various Reynolds numbers, and tested different combinations of scaling variables to exhibit similarities between the different Reynolds number cases.

In the present work, compressible LESs of a turbulent channel flow are performed. The friction Reynolds number $Re_\tau = hu_f/\nu$ is equal to 260, with h the half width of the channel, ν the molecular viscosity, and u_f the friction velocity. The Mach number is equal to 0.5. These simulations are used to perform a grid convergence study. Once the quality of grid resolution is assessed, one of the well-resolved simulations is carried on over a longer time period, allowing analysis of fine scales in the near wall region, using power spectra densities of the streamwise velocity and of the wall pressure.

2 Numerical settings

The LESs are performed by solving the compressible Navier-Stokes equations, using low-dissipation and low-dispersion 11-points finite differences for spatial derivatives. Periodic boundary conditions are implemented in the x (streamwise) and z (spanwise) directions. In the y (wall normal) direction, a no-slip boundary condition is imposed. The box dimensions are $L_x \times L_y \times L_z = 12h \times 2h \times 6h$. The dissipative effects of the subgrid motions are modelled by the use of an explicit filter of order 6, removing the smallest discretised scales, while leaving the well-resolved scales nearly unaffected [3].

The simulations are carried out on Cartesian grids, with constant mesh spacings in the streamwise and spanwise directions. In the wall normal direction, the mesh spacing is stretched with a constant expansion rate r. Grid convergence is carried out by performing simulations on several grids with decreasing mesh spacings in one direction. Two series of grids, referred to as Gdz and Gdx, are used to study the grid convergence in the z and x directions, respectively. For grid convergence in the y direction (Gdy grids), the mesh spacing at the wall Δy_w is decreased, while the expansion rate r is slightly increased. The numbers of grid points n_x, n_y and n_z in the x, y and z directions, respectively, vary between the different cases, with $87 \leq n_x \leq 257$, $85 \leq n_y \leq 161$ and $129 \leq n_z \leq 385$. Table 1 shows the grid parameters of each of the cases, in wall units. It can be noted that the parameters of Gdz4 and Gdx4 are identical to those of Gdy3, therefore these three cases refer to the same simulation. Parameters from LESs of wall bounded flows with varying Reynolds numbers from Viazzo *et al.* [10], Gloerfelt [11] and Schlatter *et al.* [12] are also given for the comparison.

Time integration is performed with the explicit fourth-order Runge-Kutta scheme of Berland *et al.* [13], at a CFL number $c\Delta t/\Delta y_w = 0.83$, with Δt the time step and c the speed of sound. An additional simulation is performed on the Gdy3 grid, using a semi-implicit Runge-Kutta (SIRK) scheme recently developed by the authors [14]. With this scheme, the terms involving derivatives in the wall normal direction are computed implicitly while the other terms are computed explicitly. Thus, a higher CFL number can be reached. For the present configuration, its value is 8.7, which is ten times higher than the CFL number allowed by the explicit scheme. However, the SIRK scheme involve a quite important CPU time per iteration. Consequently, the semi-implicit simulation is about three times slower than the explicit one, for the presented case. It must be noted that a higher Reynolds number case with finer mesh at the wall should be more favorable to the efficiency of the SIRK scheme.

Table 1: Parameters of the grids used for the grid convergence study; mesh spacings are given in wall units; $\Delta x, \Delta z$: mesh spacings in the streamwise and spanwise directions; $\Delta y_w, \Delta y_c$: mesh spacings in the wall normal direction at the wall and at the center of the channel; r: stretching rate of the mesh in the wall normal direction.

Grids	Δx^+	Δz^+	Δy_c^+	Δy_w^+	r (%)
Gdy1	15	7.5	15	**3.7**	3.5
Gdy2	15	7.5	15	**1.9**	4.0
Gdy3	15	7.5	15	**0.95**	4.4
Gdy4	15	7.5	15	**0.47**	4.5
Gdz1	15	**15**	15	0.95	4.4
Gdz2	15	**12.5**	15	0.95	4.4
Gdz3	15	**10**	15	0.95	4.4
Gdz4(=Gdy3)	15	**7.5**	15	0.95	4.4
Gdz5	15	**5**	15	0.95	4.4
Gdx1	**45**	7.5	15	0.95	4.4
Gdx2	**35**	7.5	15	0.95	4.4
Gdx3	**30**	7.5	15	0.95	4.4
Gdx4(=Gdy3)	**15**	7.5	15	0.95	4.4
Viazzo *et al.* [10]	31.4	15.7	51.84	0.88	
Gloerfelt [11]	37	14.7		0.98	2
Schlatter *et al.* [12]	25.3	10.8	14.2	<1	

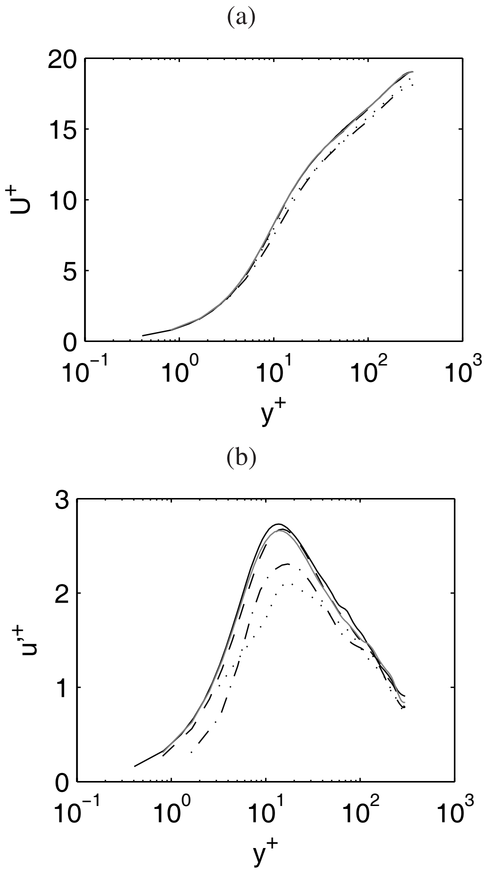

Figure 1: Grid convergence in the y direction: (a) mean, and (b) rms streamwise velocities. ······ Gdy1 ($\Delta y_w^+ = 3.7$), – · – Gdy2 ($\Delta y_w^+ = 1.9$), – – – Gdy3 ($\Delta y_w^+ = 0.95$), —— Gdy4 ($\Delta y_w^+ = 0.47$), —— Gdy3 ($\Delta y_w^+ = 0.95$) using the semi-implicit time integration scheme (SIRK)

3 Results of the grid convergence study

Profiles of mean and rms streamwise velocities are represented as a function of the distance to the wall. Figure 1 shows the results obtained with the Gdy grids, in which Δy_w^+ varies. The profiles of the Gdy3 and Gdy4 simulations are seen to collapse, for both mean and rms velocities. Therefore, grid convergence seems to be achieved for $\Delta y_w^+ = 0.95$. It can be noticed that both mean and rms velocities are underestimated by the simulations using coarser resolutions. A trend can even be established between the peak rms velocity and the grid resolution: the former increases as the latter is improved, until grid convergence is reached. The velocity profiles of the simulation performed with the SIRK scheme are also plotted. They show good agreement with those from the explicit simulation carried out on the same grid.

The velocity profiles from the Gdz grids, in which Δz^+ varies, are presented on figure 2. They show that grid convergence is obtained in Gdz3 for $\Delta z^+ = 10$. Unlike the previous case, the under-resolved simulations overestimate the mean and rms velocities, although the variations are less important here.

The results of the Gdx grids, in which Δx^+ varies, are finally plotted on figure 3. The rms velocity profiles of Gdx3 and Gdx4 collapse. Hence, grid convergence is reached for $\Delta x^+ = 30$. In the same way as for the Gdz grids, an overestimation of the mean and rms velocities is observed in the under-resolved cases.

This grid convergence study finally suggests that minimal resolutions of approximately $\Delta x^+ = 30$, $\Delta y^+ = 1$ and $\Delta z^+ = 10$ are necessary to perform a proper simulation with the considered LES approach.

4 Spectral analysis of pressure and velocity fluctuations

4.1 Definition

For spectral analysis, the simulation on the Gdy3 grid is performed further and data are stored over a time period of $T = 38h/U_c$, with U_c the centerline velocity. Added to the time of the grid convergence simulation, this yields a total duration of simulation equal to $T_{total} = 140h/U_c$. Every 40$^{\text{th}}$ time step, samples of the pressure at the walls, and of velocity components in wall-parallel planes are collected. The location of these planes are $y^+ = 13$ and 78 in wall units, and $y/h = 0.05$ and 0.3 in outer units. The location of the first plane corresponds to that of the maximum rms velocity. Therefore, the database contains time-space samples, noted $q(x_i, z_j, t_n)$; $1 \le i \le n_x$; $1 \le j \le n_z$; $1 \le n \le N$, where $N = 1300$ is the number of time samples. The quantity q represents either the wall pressure, or a velocity component in one of the planes where data is collected. For each of these vari-

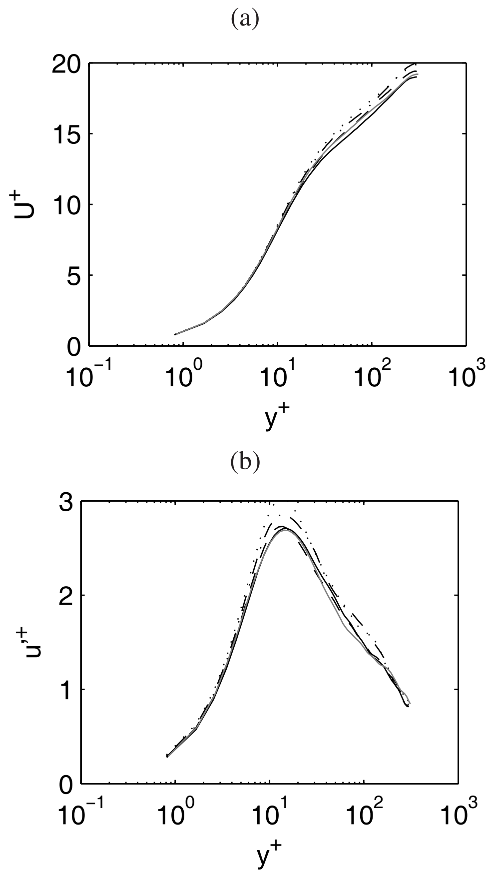

Figure 2: Grid convergence in the z direction: (a) mean, and (b) rms streamwise velocities. ······· Gdz1 ($\Delta z^+ = 15$), — · — · Gdz2 ($\Delta z^+ = 12.5$), — — — Gdz3 ($\Delta z^+ = 10$), ——— Gdz4 ($\Delta z^+ = 7.5$), ——— Gdz5 ($\Delta z^+ = 5$).

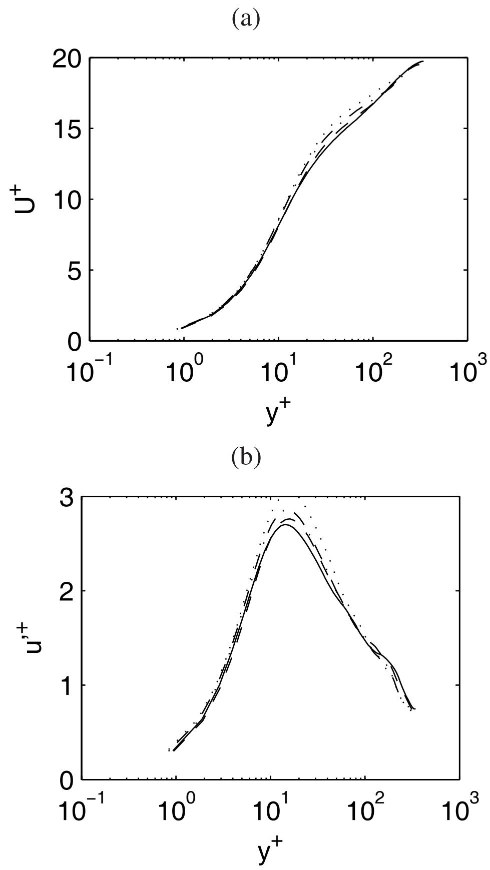

Figure 3: Grid convergence in the x direction: (a) mean, and (b) rms streamwise velocities. ······· Gdx1 ($\Delta x^+ = 45$), — · — · Gdx2 ($\Delta x^+ = 35$), — — — Gdx3 ($\Delta x^+ = 30$), ——— Gdx4 ($\Delta x^+ = 15$).

ables, a three-dimensional spectrum $\hat{q}(k_x, k_z, \omega)$ is obtained, as a function of streamwise and spanwise wavenumbers k_x and k_z, and angular frequency ω. In order to render the spectrum smoother, the database is subdivided into 9 overlapping time segments of length $N_S = 260$ ($T_S = 7.7h/U_c$). Spectra are then computed on each segment, and averaging over all the spectra gives the final 3-D spectrum. Power spectral densities (PSD) are finally obtained as $\Phi_{qq} = \hat{q}\hat{q}^*/(L_x L_z T_S)$.

The frequency range is $0.059 \leq \omega^+ = \omega\nu/u_f^2 \leq 7.7$, and the wavenumber ranges are $0.002 \leq k_x^+ = k_x\nu/u_f \leq 0.26$ and $0.004 \leq k_z^+ = k_z\nu/u_f \leq 0.51$.

4.2 Wall pressure spectra

The wall pressure frequency spectrum Φ_{pp}, shown on figure 4, is obtained by integration of the 3-D spectrum over k_x and k_z. The axes are in logarithmic scales, and coordinates are given in wall units. The spectrum has been premultiplied by the angular frequency ω to highlight the separation between high and low frequency regions. For low frequencies, the premultiplied spectrum increases with ω, following a power law with an exponent close to 1. The spectrum reaches a peak at a non-dimensional angular frequency $\omega^+ = 0.3$, as it was observed by Hu [9] for Reynolds numbers between 360 and 1440. Then, for higher frequencies, the spectrum rapidly decreases. A slope of order ω^{-4} can be noticed in a small range of frequencies $\omega^+ \approx 0.8-1$, which is consistent with the decay in ω^{-5} observed for Φ_{pp} in a number of boundary layer experiments [16]. The decay becomes sharper for $\omega^+ \geq 1$, which can be attributed to the dissipative effect of the relaxation filter of the LES, whose cut-off wavenumber is $k_x \approx 2\pi/(4\Delta x)$ in the streamwise direction. Assuming Taylor hypothesis of frozen turbulence convected at a speed roughly equal to $0.5U_c$, the non-dimensional cut-off angular frequency is equal to $\omega\nu/u_\tau^2 \approx 1.2$, which corresponds well to the frequency at which a strong decrease is observed in the figure.

Finally, a narrow peak can be seen at a frequency $\omega^+ = 0.71$, which is very close to the frequency $f_0 = c/(2h)$. A wavenumber-frequency spectrum (not shown here, for the sake of conciseness) reveals that this peak is located at wavenumbers equal to zero in the streamwise and spanwise directions, meaning that it is caused by a phenomenon which has infinite size in the homogeneous directions of the flow. Therefore, it can be stated that this peak is due to the resonance of an acoustic mode propagating perpendicularly to the wall.

4.3 Velocity spectra and spanwise structures

Figure 5 shows the power spectral densities of the three components of velocity in the plane located at $y^+ = 13$, as functions of the spanwise wavenumber, scaled by the boundary layer thickness $\delta = 0.9h$. The axes are in logarithmic scales. At low frequencies, the levels found in the spectrum for the wall-normal velocity are around two orders of magnitude lower than that for the spanwise velocity. The latter is one order of magnitude lower than that for the streamwise

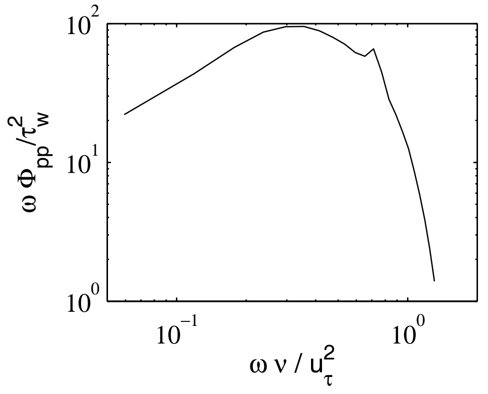

Figure 4: Premultiplied power spectral density of the fluctuating wall pressure scaled by the wall shear stress, as a function of the angular frequency, scaled by the viscous time scale

velocity over the whole range of wavenumbers. These differences indicate the strong anisotropy of the velocity fluctuations in the near-wall region. The spectrum of the streamwise velocity spreads over a large range of wavenumbers, but the maximum is found at $k_z\delta \approx 8$. A peak is found also for the wall normal velocity component, around $k_z\delta \approx 16$. This spatial arrangement is a typical feature of the near-wall streaks, which consist in regions of high and low streamwise velocity elongated in the streamwise direction. These structures are arranged regularly in the spanwise direction, giving the observed peak in the spanwise spectrum. The streaks are accompagnied by streamwise vortices, whose spanwise separation is twice smaller than that of the streaks. These vortices induce the peak visible in the spectrum of the wall normal velocity.

It can be noticed that the spanwise separation of the streaks is slightly higher than the size of 100 wall units usually observed in the literature [15]. Indeed, the peak at $k_z\delta \approx 8$ observed for the streamwise velocity corresponds to a wavelength $\lambda_z^+ = 180$. A similar shift has been noted by Tomkins & Adrian [4] in boundary layers at $Re_\tau = 426$, with the most energetic scales ranging over $200 \leq \lambda_z^+ \leq 400$ at $y^+ = 21$.

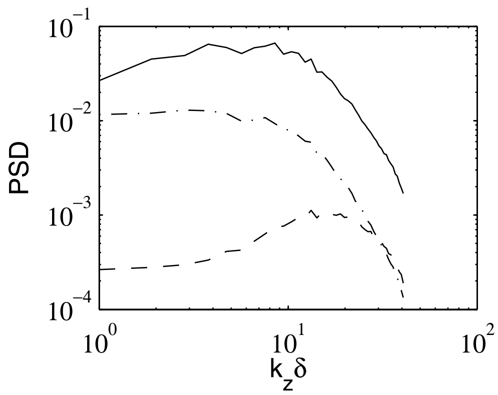

Figure 5: Power spectral densities of velocity fluctuations, at a distance to the wall $y^+ = 13$, as a function of the spanwise wavenumber scaled by the boundary layer thickness $\delta = 0.9h$: ——— Φ_{uu}, – – – Φ_{vv}, – · – · Φ_{ww}.

The spectra obtained from the data further from the wall, at $y^+ = 78$, or $y = 0.3\delta$ in outer units, are presented in the figure 6. The velocity field is observed to be more isotropic than previously. Anisotropy however persists at low wavenumbers, since wall normal components of the velocity are less energetic than streamwise components for $k_z\delta < 7$. The spectrum is dominated by lower wavenumbers compared to the near wall spectrum. Indeed, a peak is located at $k\delta \approx 3$, corresponding to a wavelength $\lambda_z \approx 2\delta$. This value is higher than that provided by Tomkins & Adrian from boundary layer experiments, who measured the most energetic scales around $\lambda_z \approx 0.8\delta$, at $y = 0.2\delta$ [4]. However, the authors pointed out that the largest scales of boundary layers and channel flows should exhibit different behaviors, since they are influenced by the geometry of the facility.

Comparison can also be made with the LES results of Bogey *et al.* for a tripped nozzle pipe flow [6]. Just downstream of the exit, the azimuthal modes of the streamwise velocity are noticed to be the most energetic at $k_\theta\delta/r_0 \approx 7$ [7], where r_0 is the pipe radius.

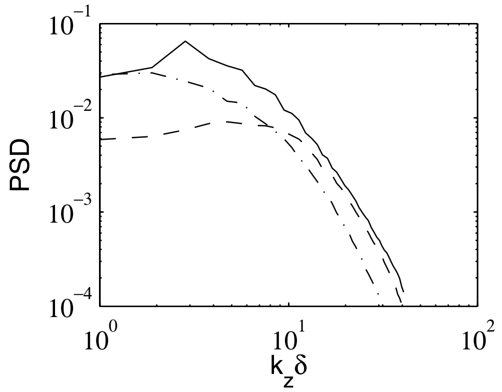

Figure 6: Power spectral densities of velocity fluctuations, at a distance to the wall $y = 0.3\delta$, as a function of the spanwise wavenumber scaled by the boundary layer thickness $\delta = 0.9h$: ——— Φ_{uu}, – – – Φ_{vv}, – · – · Φ_{ww}.

Finally, a two dimensional spectrum of the streamwise velocity at $y^+ = 13$ is shown on figure 7 as a function of the spanwise and streamwise wavenumbers given in wall units. It is clearly visible that the energy is concentrated in the low streamwise wavenumbers, suggesting an important elongation of the streaks in the streamwise direction. As previously, dominant componants are found for $0.008 \leq k_z^+ \leq 0.04$, corresponding to $150 \leq \lambda_z^+ \leq 780$. The separation of $\lambda_z^+ = 100$ usually observed for the streaks corresponds to $k_z^+ = 0.063$. Energetic components can be noticed for this value of wavenumber, suggesting that streaks with a spanwise separation of 100 wall units are present, but that they are less energetic than the dominant ones. It can also be remarked that for this value of k_z^+, the spectrum is spread over larger values of k_x^+.

5 Conclusion

A grid convergence study is performed to evaluate the minimal resolution necessary to obtain a well resolved LES for a turbulent channel flow at $Re_\tau = 260$. It is found that relatively small mesh spacings are necessary, namely $\Delta x^+ = 30$, $\Delta y_w^+ = 1$ and $\Delta z^+ = 10$, which however remain higher than those of a DNS resolution. One of the well resolved simulations is used to compute spectral data on which further ana-

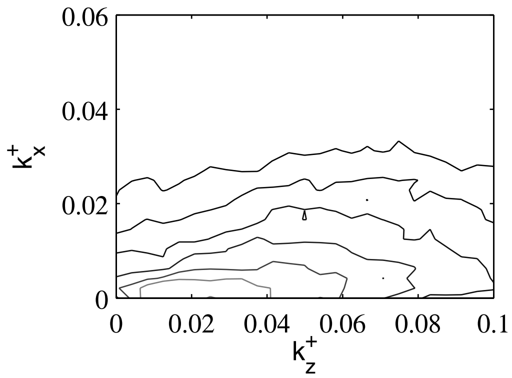

Figure 7: Power spectral density of the streamwise velocity fluctuations Φ_{uu}, at a distance to the wall $y^+ = 13$, as a function of the streamwise (k_x) and spanwise (k_z) wavenumbers, given in wall units. Two consecutive isolines represent a magnitude ratio of 2.

lyses are carried out. The wall pressure frequency spectrum is consistent with that provided by Hu *et al.* [9]. Near wall streaks are studied using spanwise spectra of velocity components, which show that the streaks have a spanwise separation of roughly 180 wall units, supporting the observations of Tomkins & Adrian [4]. Further from the wall, the turbulent structures exhibit quite high separations, around $\lambda_z \approx 2\delta$.

As a concluding remark, the well resolved LES shows the ability to produce relieable results, for a lower computation cost compared to DNS. The resolution of DNS for wall-bounded flow is indeed about twice as high in each direction, resulting in a number of grid points 8 times higher than that of LES. Assuming the use of the same time integration scheme, computational time is then 16 times longer.

Acknowledgments

This work was granted access to the HPC resources of the Institut du Développement et des Ressources en Informatique Scientifique (IDRIS) under the allocation 2011-020204 made by GENCI (Grand Equipement National de Calcul Intensif). It was granted financial support by the Direction Générale de l'Armement (DGA) and the Centre National de la Recherche Scientifique (CNRS).

References

[1] J. Kim, P. Moin, R. Moser. "Turbulence statistics in fully developed channel flow at low Reynolds number", *Journal of Fluid Mechanics* **177**, 133-166 (1987)

[2] P. Schlatter, R. Orlu. "Assessment of direct numerical simulation data of turbulent boundary layers", *Journal of Fluid Mechanics* **659**, 116-126 (2010)

[3] C. Bogey, C. Bailly. "Large eddy simulations of transitional round jets: Influence of the Reynolds number on flow development and energy dissipation", *Physics of Fluids* **18**, 065101 (2006)

[4] C.D. Tomkins, R.J. Adrian. "Energetic spanwise modes in the logarithmic layer of a turbulent boundary layer", *Jounal of Fluid Mechanics* **545**, 141-162 (2005)

[5] J. Jiménez, S. Hoyas, M. Simens, Y. Mizuno. "Turbulent boundary layers and channels at moderate Reynolds numbers", *Journal of Fluid Mechanics* **657**, 335-360 (2010)

[6] C. Bogey, O. Marsden, C. Bailly. "Large-eddy simulation of the flow and acoustic fields of a Reynolds number 10^5 subsonic jet with tripped exit boundary layers", *Physics of Fluids* **23**, 035104 (2011)

[7] C. Bogey, O. Marsden, C. Bailly. "On the spectra of nozzle-exit velocity disturbances in initially nominally turbulent, transitional jets", *Physics of Fluids* **23**, 091702 (2011)

[8] M.K. Bull. "Wall-pressure fluctuations beneath turbulent boundary layers: some reflections on forty years of research", *Journal of Sound and Vibration* **190**(3), 299-315 (1996)

[9] Z.H. Hu, C.L. Morfey, N.D. Sandham. "Wall pressure and shear stress spectra from direct simulations of channel flow", *AIAA Journal* **44**(7), 1541-1549 (2006)

[10] S. Viazzo, A. Dejoan, R. Schiestel. "Spectral features of the wall-pressure fluctuations in turbulent wall flows with and without perturbations using LES", *International Journal of Heat and Fluid Flow* **22**, 39-52 (2001)

[11] X. Gloerfelt. "The link between wall pressure spectra and radiated sound from turbulent boundary layers", *16th AIAA/CEAS AeroAcoustics Conference, AIAA Paper 2010-3904* (2010)

[12] P. Schlatter, Q. Li, G. Brethouwer, A.V. Johansson, D.S. Henningson. "Simulations of spatially evolving turbulent boundary layers up to $Re_\theta = 4300$", *International Journal of Heat and Fluid Flow* **31**, 251-261 (2010)

[13] J. Berland, C. Bogey, C. Bailly. "Low-dissipation and low-dispersion 4th-order Runge-Kutta algorithm", *Computers and Fluids*, **35**, 1459-1463 (2006)

[14] F. Kremer, C. Bogey, C. Bailly. "Étude de schémas de Runge-Kutta semi-implicites pour la simulation des écoulements de paroi", *20ème Congrès Francais de Mécanique* (2011)

[15] S.J. Kline, W.C. Reynolds, F.A. Schraub, P.W. Runstadler. "The structure of turbulent boundary layers", *Journal of Fluid Mechanics* **30**, 741-773 (1967)

[16] M.C. Goody, R.L. Simpson. "Surface pressure fluctuations beneath two- and three-dimensional turbulent boundary layers", *AIAA Journal* **38**(10), 1822-1831 (2000) "